

The decoupling problem at RHIC

Dénes Molnár¹ and Miklos Gyulassy¹

¹ Physics Department, Columbia University
538 W. 120th Street, New York, NY 10027

Abstract. We investigate whether it is possible to *dynamically* generate from classical transport theory the observed surprising $R_{out} \approx R_{side}$ in Au+Au at $\sqrt{s} = 130A$ GeV at RHIC [1, 2]. We obtained covariant solutions to the Boltzmann transport equation via the MPC technique [3], for a wide range of partonic initial conditions and opacities. We demonstrate that there exist transport solutions that yield a freezeout distribution with $R_{out} < R_{side}$ for $K_{\perp} > \sim 1.5$ GeV. These solutions correspond to continuous evaporation-like freezeout, where the emission duration is *comparable* to the source size. Naively this would mean $R_{out} > R_{side}$. Nevertheless, our sources exhibit $R_{out} < R_{side}$ because they are narrower in the 'out' than in the 'side' direction and, in addition, a positive $x_{out} - t$ correlation develops reducing R_{out} further.

Keywords: HBT interferometry, freezeout, transport theory, RHIC

PACS: 12.38.Mh; 24.85.+p; 25.75.-q; 25.75.Gz

1. Introduction

Long-standing theoretical interests of the RMKI KFKI research group have been hydrodynamical, decoupling and transport phenomena [4, 5, 6, 7]. A recent theoretical puzzle is why the pion source extracted via HBT interferometry in Au+Au at $\sqrt{s} = 130A$ GeV at RHIC has approximately identical 'out' and 'side' radii for average pair momenta $K_{\perp} < 0.7$ GeV [1, 2]. Most naively, this indicates very short pion emission duration, corresponding to almost instantaneous decoupling.

The observed ratio $R_{out}/R_{side} \approx 0.9 - 1.1$ contradicts theoretical expectations based on cylindrically symmetric and longitudinally boost invariant ideal hydrodynamics, indicating R_{out}/R_{side} significantly larger than one [8, 9]. On the other hand, a hydrodynamical approach to the decoupling problem is inherently questionable because in the decoupling region the mean free path exceeds the side of the system, while hydrodynamics is only valid if the mean free path is zero. As a workaround, hydrodynamics is usually supplemented with an *arbitrary* freeze-

out prescription postulating sudden freezeout on a three-dimensional hypersurface, which is typically parametrized by a constant freezeout temperature or energy density. The unsatisfactory nature of this procedure has been realized recently and several improvements have been proposed [5].

A dynamical framework with a self-consistent freezeout is provided by classical transport theory[10, 11, 12, 3, 13], where the rate of interactions is given by the product of the density and the cross section $\lambda^{-1} = n\sigma$. As the system expands, it rarifies, and the rate of particle interactions drops accordingly. Because the theory is not limited to equilibrium dynamics, it also allows for systematic studies of dissipative effects. Dissipation is crucial in order to reproduce[3] the observed saturation of elliptic flow at $p_{\perp} > 2$ GeV[14].

The equilibrium assumption was partly relaxed in an earlier study[15], where hydrodynamical evolution was only assumed until hadronization at which point particles were fed into a hadronic cascade. The calculation gave $R_{out}/R_{side} \approx 1.2 - 1.4$, still above one. On the other hand, it is not clear whether the hadronic densities were large enough to support equilibrium on the freezeout hypersurface, which would be necessary to justify the assumed equilibrium evolution until the end of hadronization. In fact, antiprotons are known to scatter only once on average in this approach, indicating the need for a nonequilibrium approach before hadronization.

In this study we investigate how nonequilibrium evolution in the partonic phase influences the pion distributions at freezeout. Utilizing the MPC numerical technique[16], we compute the covariant freezeout distributions for a variety of initial conditions for Au+Au at $\sqrt{s} = 130A$ GeV based on perturbative QCD, gluon saturation models, or a combination of both. Varying the transport opacity, which is an effective measure of the degree of collectivity[3], we study under what conditions $R_{out} < R_{side}$ is possible.

2. Two-particle HBT interferometry

Hanbury-Brown and Twiss interferometry is a truly remarkable technique to deduce *space-time* geometrical information purely via measuring momentum correlations. We review here only a few essential features and refer the reader to Refs. [17, 7, 18] and references therein.

Detailed studies of pion production by an ensemble of classical currents[17] showed that for a chaotic boson source $\rho(\vec{x}, t)$, in the limit of a large particle numbers, and also neglecting final state interactions, the two-particle correlation function is given by the *space-time* Fourier transform of the source as

$$C(q, K) \equiv C(p_1, p_2) \equiv \frac{N(p_1, p_2)}{N(p_1)N(p_2)} = 1 + \left| \int d^4x \rho(\vec{x}, t) e^{iqx} \right|^2. \quad (1)$$

Here $q^{\mu} \equiv p_1^{\mu} - p_2^{\mu}$ is momentum difference, while $K^{\mu} \equiv (p_1^{\mu} + p_2^{\mu})/2$ is the average momentum of the boson pair.

Unfortunately, Eq. (1) cannot be uniquely inverted to obtain the source distribution, because the phase information is lost and, in addition, only a three-

dimensional projection of the four-dimensional correlation function is measurable because q^μ is constrained[18] by

$$q^\mu K_\mu = (m_1^2 - m_2^2)/2 = 0 \quad (\text{for identical particles}) . \quad (2)$$

Despite the inversion problem, HBT measurements provide strong constraints on the freezeout distributions of particles and therefore on the possible dynamical scenarios in heavy-ion collisions.

Conventionally, $C(\vec{q}, K)$ is expressed in terms of the 'out-side-long' variables, q_O , q_S , and q_L . These are defined in the longitudinally boosted LCMS reference frame, where $K_z = 0$ with z or 'long' being the beam direction, 'out' the direction of \vec{K}_\perp , and 'side' the one orthogonal to both. In this frame, $K_{LCMS}^\mu = (\tilde{K}^0, K_\perp, 0, 0)$, $\vec{q}_{LCMS} = (q_O, q_S, q_L)$, $x_{LCMS}^\mu \equiv (\tilde{t}, x_O, x_S, x_L)$ and Eq. (2) gives

$$q^\mu x_\mu = -q_O(x_O - \tilde{t}K_\perp/\tilde{K}^0) - q_S x_S - q_L x_L . \quad (3)$$

Clearly, the measurable projected correlation function is completely blind to the dependence of the source function on the fourth orthogonal coordinate $\tilde{t} + x_O K_\perp / \tilde{K}^0$.

Experimentally, the measured correlation function (after correcting for final state interactions) is fitted with a Gaussian, which for central collisions ($b = 0$) and at midrapidity is constrained by symmetry to be of the form

$$C(\vec{q}, K) = \lambda(K) \exp[-q_O^2 R_O^2(K) - q_S^2 R_S^2(K) - q_L^2 R_L^2(K)] . \quad (4)$$

Here R_O , R_S and R_L are the 'out', 'side', and 'long' HBT radii. For a *perfectly Gaussian* source, the correlation function is Gaussian and

$$\begin{aligned} R_O^2(K) &= \langle \Delta x_O^2 \rangle_K + v_\perp^2 \langle \Delta \tilde{t}^2 \rangle_K - 2v_\perp \langle \Delta x_O \Delta \tilde{t} \rangle_K \\ R_S^2(K) &= \langle \Delta x_S^2 \rangle_K, \quad \text{and} \quad R_L^2(K) = \langle \Delta x_L^2 \rangle_K , \end{aligned} \quad (5)$$

where $v_\perp \equiv K_\perp / \tilde{K}^0$. Thus R_S and R_L have simple geometric interpretation as the 'side' and 'long' widths of the distribution function, while R_O is a mixture of the 'out' width, time spread, *and* the $x_O - \tilde{t}$ correlation.

3. Covariant parton transport theory

3.1. Transport equation

We consider here, as in Refs. [10, 11, 12, 3], the simplest but nonlinear form of Lorentz-covariant Boltzmann transport theory in which the on-shell phase space density $f(x, \vec{p})$, evolves with an elastic $2 \rightarrow 2$ rate as

$$p_1^\mu \partial_\mu f_1 = S(x, \vec{p}_1) + \iiint_{234} (f_3 f_4 - f_1 f_2) W_{12 \rightarrow 34} \delta^4(p_1 + p_2 - p_3 - p_4) . \quad (6)$$

Here W is the square of the scattering matrix element, the integrals are shorthands for $\int \equiv \int \frac{g d^3 p_i}{(2\pi)^3 E_i}$, where g is the number of internal degrees of freedom, while $f_j \equiv f(x, \vec{p}_j)$. The initial conditions are specified by the source function $S(x, \vec{p})$. For our applications below, we neglect quark degrees of freedom and interpret $f(x, \vec{p})$ as describing an ultrarelativistic massless gluon gas with $g = 16$ (8 colors, 2 helicities).

The elastic gluon scattering matrix elements in dense parton systems were modeled with the isotropic form $d\sigma_{el}/dt = \sigma_0(s)/s$. The simplified angular dependence is justified by our previous study[3], where we showed that the covariant transport solutions do not depend *explicitly* on the differential cross section but only on the *transport opacity*

$$\chi \equiv \frac{\sigma_{tr}}{\sigma_{el}} \langle n \rangle \approx \sigma_{tr} \langle \int dz \rho(\mathbf{x}_0 + z\hat{\mathbf{n}}, \tau = \frac{z}{c}) \rangle . \quad (7)$$

Here

$$\sigma_{tr}(s) \equiv \int d\sigma_{el} \sin^2 \theta_{cm} = \int dt \frac{d\sigma_{el}}{dt} \frac{4t}{s} \left(1 - \frac{t}{s}\right) \quad (8)$$

is the transport cross section (in our case, $\sigma_{tr} = 2\sigma_0/3$), while $\langle n \rangle$ is the average number of scatterings a parton undergoes. We neglected the weak logarithmic energy dependence of the total cross section and took a constant σ_0 for simplicity. For a fixed nuclear geometry, a given transport opacity χ represents a whole class of initial conditions and partonic matrix elements, which is demonstrated by the approximate proportionality[3] $\chi \propto \sigma_{tr} dN_g(\tau_0)/d\eta$.

We solved Eq. (6) numerically via the MPC parton cascade algorithm [16], which utilizes the parton subdivision technique[10, 11] to obtain the correct, covariant solutions to the transport equation. Parton subdivision is essential to eliminate numerical artifacts caused by acausal (superluminal) propagation due to action at a distance[12]. For initial partonic densities expected at RHIC, the severe violation of Lorentz covariance in the naive cascade algorithm that employs no subdivision artificially reduces elliptic flow and heats up the p_\perp spectra[3, 13].

3.2. Initial conditions

We modeled central Au+Au collisions at RHIC with three different classes of initial conditions, corresponding to different assumptions on the initial transverse momentum distribution and density distribution of partons. In all three cases, the evolution started from a longitudinally boost invariant Bjorken tube at proper time $\tau_0 = 0.1$ fm/c, with isotropic momentum distribution in the local rest frame and with uniform pseudorapidity $\eta \equiv 1/2 \log[(t+z)/(t-z)]$ distribution between $|\eta| < 5$.

The first class was essentially the same as the minijet initial conditions in Ref. [3]. The initial transverse density distribution was proportional to the binary collision distribution for two Woods-Saxon distributions, while the p_\perp distribution was a fit to the minijet distribution predicted by HIJING[19] (without shadowing and jet quenching). To include the transport effect of the soft partonic component

present in HIJING *in addition* to the minijets, in the present study we increased the parton density by a factor five, to yield $dN_g(\tau_0)/d\eta = 1000$.

The second class was based on gluon saturation models. Here we assumed a uniform Bjorken cylinder with a radius $R_0 = 6$ fm, $dN_g/d\eta = 1000$ and a constant $d^2N/p_\perp dp_\perp$ distribution that vanishes for $p_\perp > Q_{sat} = 1.2$ GeV.

The third class was a combination of the first two. We took the minijet part with the original HIJING normalization ($dN/d\eta = 210$) and added four times as many saturated soft gluons.

4. Results

Using MPC, we computed the freezeout distribution numerically for central Au+Au at 130A GeV as a function of the average pair momentum and transport opacity, for all three classes of initial conditions.

The freezeout distribution d^4N/d^4x was defined as the distribution of space-time coordinates for the point of last interaction of the test particles, with the strong assumption that this point is not affected by hadronization. We furthermore neglected resonance contributions to the pion yield. The same two hadronization schemes, parton-hadron duality and independent fragmentation, were applied as in Ref. [3].

Of our primary interest were the integrated distributions $d^2N/rdrd\tilde{t}$, the equivalent of the usual hydrodynamical freezeout curves in the $r-\tau$ plane, and $d^2N/dx_O dx_S$, which is the source projected onto the 'out-side' plane. We worked in the approximation $p_{1,\perp} \approx p_{2,\perp} \approx K_\perp$, which is valid up to corrections of $O(|\vec{q}|/|\vec{K}|)$. To get a simple estimate of the radii, we used Eq. (5) even though our sources are non-Gaussian. A more detailed analysis of the radii based on the momentum-space correlation function is in progress.

Figure 1 shows the freezeout distribution in $r - \tilde{t}$ coordinates ($r \equiv \sqrt{x_O^2 + x_S^2}$) as a function of the pair momentum and transport opacity for the minijet initial condition with hadronization via parton-hadron duality. Unlike the sharp freezeout imposed in hydrodynamical models, the transport theory freezeout is a continuous [12], *evaporation-like* process. For a given (nonzero) opacity, the larger the p_\perp of the particle, the earlier it decouples and the closer it is to the surface of the nuclei. Thus, low- p_\perp partons freeze out in the center at late times, while high- p_\perp ones escape from the surface at early times. Furthermore, a larger opacity increases decoupling times, especially for low- p_\perp particles. We observed the same features for the other two classes of initial conditions.

Figure 2 shows the shape of the source in $x_O - x_S$ coordinates as a function of the pair momentum and transport opacity for the minijet initial condition with hadronization via parton-hadron duality. Results for the saturation and the 'combined' initial condition were very similar. The black crosses are positioned at the first moment of the distributions ($\langle x_O \rangle, \langle x_S \rangle$), while their extension corresponds to the square root of the second moments ($\sqrt{\langle \Delta x_O^2 \rangle}, \sqrt{\langle \Delta x_S^2 \rangle}$). As the opacity in-

creases, the source shrinks in the 'out' direction and the higher the p_{\perp} , the more pronounced the reduction of $\langle \Delta x_O^2 \rangle$ is. From Eq. (5) it is clear that this will help reduce R_O , at least if the other two terms do not change. On the other hand, we find that the source size in the 'side' direction is approximately independent of both the opacity and p_{\perp} . Thus, surprisingly, R_S is unaffected by the strong collective dynamics.

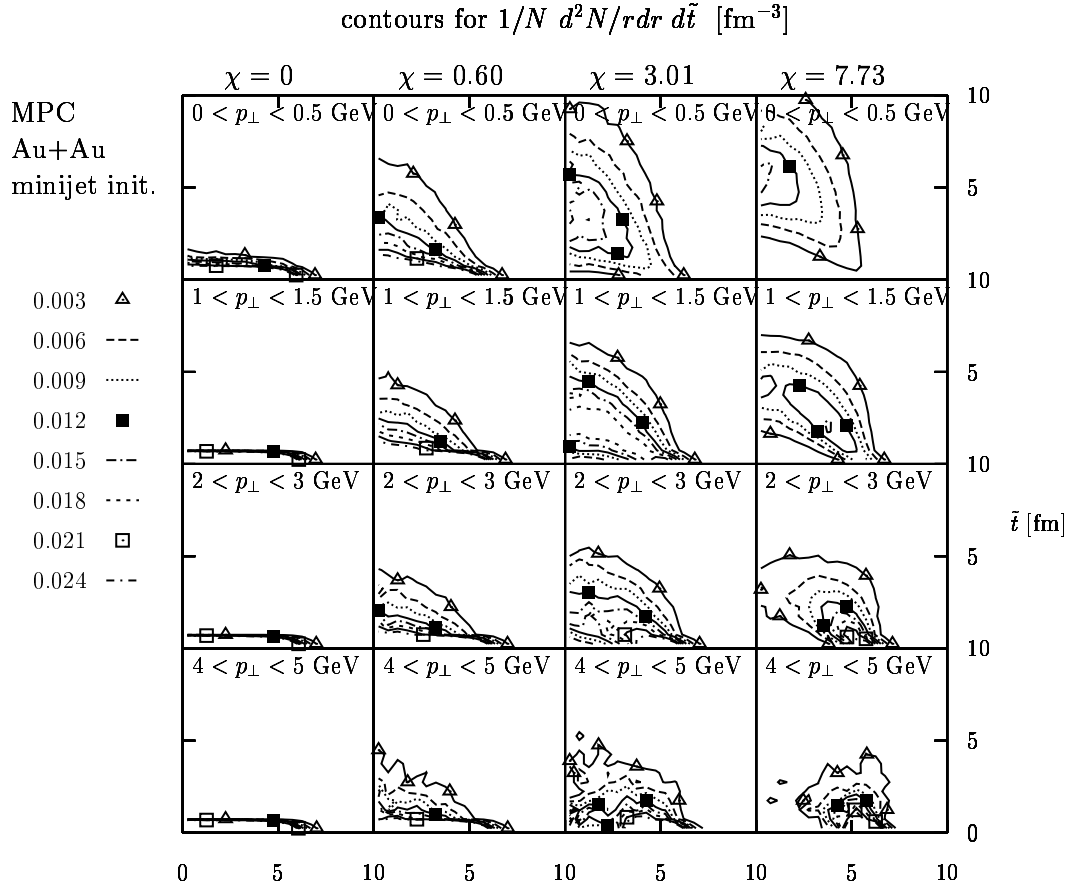


Fig. 1. Freezeout $r - \tilde{t}$ distribution as a function of transport opacity and p_{\perp} for the minijet initial condition with hadronization via parton-hadron duality.

The mean $\langle x_O \rangle$ does not coincide with the maximum of the distributions showing that the distributions are asymmetric in the 'out' direction, i.e., they are clearly non-Gaussian. In fact, the change in the shape of contour lines with increasing opacity is much more pronounced than the slow decrease of the second moment $\langle \Delta x_O^2 \rangle$ because there is a long tail in the negative 'out' direction. We expect that R_O extracted via a least-squared Gaussian fit would turn out to be somewhat *smaller*

than from Eq. (5).

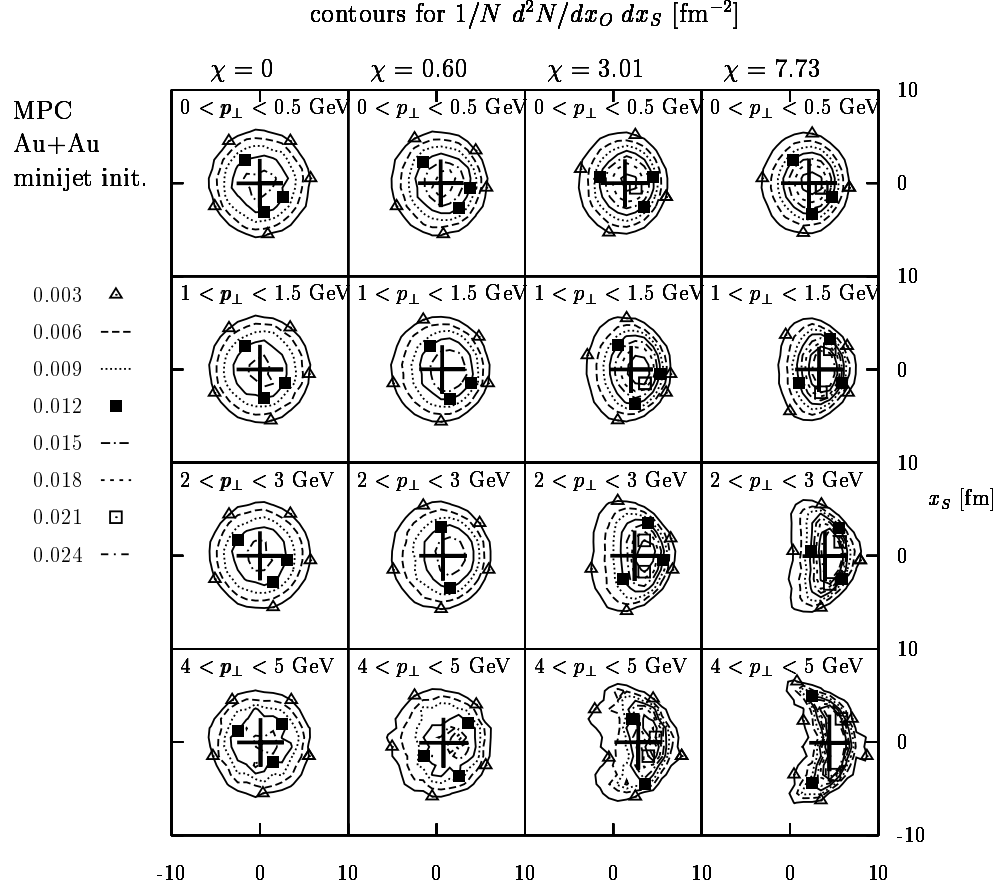


Fig. 2. Freezeout $x_O - x_S$ distribution as a function of transport opacity and K_\perp for the minijet initial condition with hadronization via parton-hadron duality.

The left column in Fig. 3 shows the dependence of the R_O/R_S and R_L/R_O ratios on transport opacity and K_\perp for the minijet initial condition. For $\chi = 0$, both R_O and R_S are determined by the nuclear size to be ≈ 3 fm, therefore $R_O/R_S = 1$. However, as the opacity increases, the ratio increases above one for $K_\perp < K_c$, while decreases below one for $K_\perp > K_c$, where the location of the turning point $K_c \approx 1.3 - 2$ GeV depends on the hadronization scheme.

The naive $R_O^2 = R_S^2 + \Delta t^2$ expectation does not hold now because in the LCMS frame the source is not cylindrical (see Fig. 2) and there are dynamical correlations. Figure 4 illustrates how the different terms in Eq. (5) contribute to R_O as a function of K_\perp . For all three classes of initial conditions, the time spread $\langle \Delta t^2 \rangle$ is comparable to the spatial width of the source ~ 3 fm, which has the effect

to increase R_O . However, this effect is compensated by the large *positive* $x_O - \tilde{t}$ correlation term, reducing R_O below R_S .

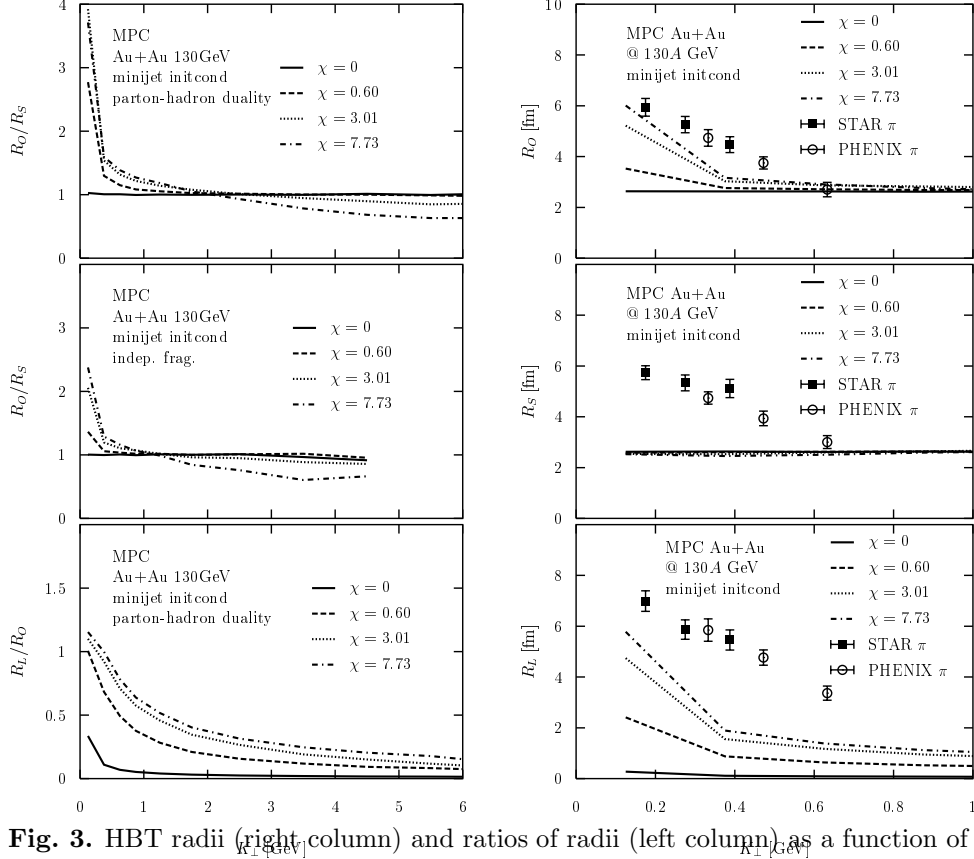


Fig. 3. HBT radii (right column) and ratios of radii (left column), as a function of transport opacity and K_{\perp} for the minijet initial condition, with hadronization via parton-hadron duality (top and middle left) or independent fragmentation (bottom left and whole right column).

The right column in Fig. 3 shows a comparison to the HBT radii measured at RHIC. In the transverse opacity range $\chi \sim 0 - 8$ we studied, the transport theory results are smaller than the observed R_O and R_L . This is in sharp contrast to ideal hydrodynamics, which overpredicts both radii [9]. The monotonic dependence of R_O and R_L on opacity indicates that a much better agreement with the data is possible at a larger but *finite* opacity $\chi > \sim 10$.

In Fig. 3, the reason for the anomalous small R_L for zero opacity is instantaneous freezeout at the formation time $\tau = \tau_0$. Since $R_L^2 \approx \tau^2 [\Delta(\eta - y)]^2$, R_L depends on the decoupling time and the strength of the $\eta - y$ correlation. For our

thermally correlated initial condition $[\Delta(\eta - y)]^2 \approx T/m_\perp$ and $\tau_0 = 0.1$ fm/c, which for $\chi = 0$ gives $R_L < \approx 0.5$ fm for all K_\perp bins we studied.

However, as the transport opacity increases, R_L becomes much larger because the decoupling time increases as is evident from Fig. 1. The largest increase $\tau/\tau_0 \sim R/\tau_0 \sim 50$ is for low- p_\perp partons, which freeze out latest. Thus the observed $R_L(K_\perp)$ carries important constraints on the dynamics of freezeout. For example, perfect inside-outside correlation, i.e., $\eta = y$ as assumed in classical Yang-Mills approaches cannot be reconciled with the RHIC data because it gives $R_L = 0$.

Finally, the biggest puzzle in Fig. 3 is why $R_S(K_\perp) \approx \text{const} \approx 3$ fm contrary to the data and furthermore independent of the transport opacity. This suggests that R_S is independent of the degree of collective dynamics, i.e., it is determined solely by the initial nuclear geometry. The same problem with R_S being too small and insensitive to the dynamical assumptions has been observed in hydrodynamical calculations as well [9].

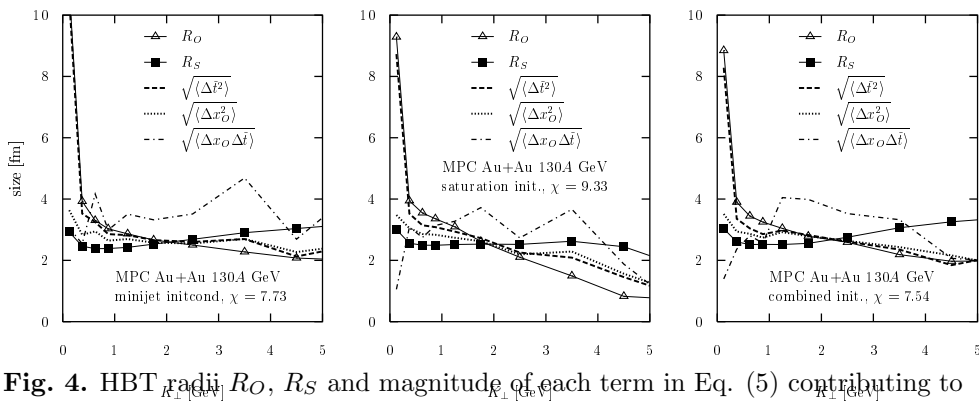


Fig. 4. HBT radii R_O , R_S and magnitude of each term in Eq. (5) contributing to R_O as a function of K_\perp for all three classes of initial conditions with hadronization via parton-hadron duality.

Acknowledgements

D. M. would like to acknowledge enlightening discussions with Tamás Csörgő and Ulrich Heinz.

This work was supported by the Director, Office of Energy Research, Division of Nuclear Physics of the Office of High Energy and Nuclear Physics of the U.S. Department of Energy under contract No. DE-FG-02-93ER-40764.

References

1. C. Adler *et al.* [STAR Collaboration], Phys. Rev. Lett. **87**, 082301 (2001) [nucl-ex/0107008].

2. K. Adcox *et al.* [PHENIX Collaboration], nucl-ex/0201008.
3. D. Molnar and M. Gyulassy, Nucl. Phys. A **697**, 495 (2002) [nucl-th/0104073].
4. T. S. Biro, P. Levai and J. Zimanyi, Phys. Lett. B **347**, 6 (1995).
5. V. K. Magas *et al.*, Heavy Ion Phys. **9**, 193 (1999) [nucl-th/9903045].
6. V. K. Magas, L. P. Csernai and D. D. Strottman, Phys. Rev. C **64**, 014901 (2001) [hep-ph/0010307].
7. T. Csorgo, hep-ph/0001233; A. Ster, T. Csorgo and J. Beier, Heavy Ion Phys. **10**, 85 (1999) [hep-ph/9810341].
8. D. H. Rischke and M. Gyulassy, Nucl. Phys. A **608**, 479 (1996) [nucl-th/9606039].
9. U. W. Heinz and P. F. Kolb, hep-ph/0111075.
10. Y. Pang, RHIC 96 Summer Study, CU-TP-815 preprint (unpublished); Generic Cascade Program (GCP) documentation available at WWW site <http://www.cunuke.phys.columbia.edu/rhic/gcp>.
11. B. Zhang, Comput. Phys. Commun. **109**, 193 (1998) [nucl-th/9709009].
12. D. Molnar and M. Gyulassy, Phys. Rev. C **62**, 054907 (2000) [nucl-th/0005051].
13. S. Cheng *et al.*, Phys. Rev. C **65**, 024901 (2002) [nucl-th/0107001].
14. R. J. Snellings [STAR Collaboration], Nucl. Phys. A **698**, 193 (2002) [nucl-ex/0104006].
15. S. Soff, S. A. Bass and A. Dumitru, Phys. Rev. Lett. **86**, 3981 (2001) [nucl-th/0012085].
16. D. Molnár, MPC 1.5.9. This parton cascade code used in the present study can be downloaded from WWW at <http://www.cunuke.phys.columbia.edu/people/molnard>
17. M. Gyulassy, S. K. Kauffmann and L. W. Wilson, Phys. Rev. C **20**, 2267 (1979).
18. U. A. Wiedemann and U. W. Heinz, Phys. Rept. **319**, 145 (1999) [nucl-th/9901094].
19. M. Gyulassy and X. Wang, Comput. Phys. Commun. **83**, (1994) 307 [nucl-th/9502021].